Journal of Engineering Science and Technology
Vol. 21, No. 3 (2026) 730 - 746

SYNERGISTIC DEGRADATION OF ANILINE BY A COMBINED FERRATE/PERSULFATE SYSTEM: EFFICIENCY, MECHANISM, AND PATHWAYS

FEIHU ZENG[1,*], ZHIWEN WANG[1], RUOLAN LIN[1], SYYI SIM[2], XIANFENG HUANG[3], FENG WANG[1]

[1]Liming Vocational University, 362000, Quanzhou, China
[2]Faculty of Electrical and electronic engineering, Universiti Tun Hussein Onn Malaysia, Johor, Malaysia
[3]School of Life and Environmental Science, Wenzhou University, 325035, Wenzhou, China
*Corresponding Author: 13859765695@163.com

Abstract

Aniline, a highly toxic and refractory organic pollutant commonly found in industrial wastewater, poses significant risks to ecosystems and human health. This study systematically investigates the synergistic degradation of aniline using ferrate (Fe(VI)) and persulfate (SPS) oxidation system. The effects of key operational parameters, including SPS dosage, temperature, and initial pH were evaluated, while radical quenching experiments and LC-MS analysis were employed to identify active species and degradation intermediates. The results demonstrated that the Fe (VI)/SPS system achieved a removal efficiency of 76.41% within 30 minutes, significantly surpassing those of the individual Fe (VI) (37.78%) and SPS (33.21%), and exceeding their arithmetic sum (70.99%). Increasing SPS dosage from 10 mM to 50 mM enhanced the 60-minute degradation rate from 60% to 97.5%, and raising the temperature from 10 °C to 60 °C increased the apparent rate constant by nearly four times. Acidic conditions (pH = 3) favored faster degradation, with •OH and SO_4•$^-$ being the predominant radicals, whereas non-radical pathways mediated by high-valent iron species (Fe (IV)/Fe(V)) dominated under alkaline conditions. Four major degradation pathways were proposed based on identified intermediates, culminating in complete mineralization. The study provides new mechanistic insights into the Fe(VI)/SPS synergistic oxidation process and offers a promising strategy for the effective treatment of aniline-laden industrial wastewater.

Keywords: Aniline, Ferrate, Persulfate, Radical, Wastewater.

1. Introduction

Aniline, a vital chemical intermediate, is extensively utilized in industries such as defense, dyeing, and pharmaceuticals. Wastewater containing aniline is designated as a Group 2B carcinogen by the International Agency for Research on Cancer (*IARC*), owing to its persistence against biodegradation and significant ecological toxicity, which threatens both environmental and human health [1].

Conventional treatment technologies face significant limitations: physical adsorption merely transfers the pollutant to another phase rather than achieving ultimate degradation [2], while biological methods exhibit limited tolerance to high concentrations of aniline [3]. Advanced oxidation processes (AOPs) have emerged as promising alternatives by generating highly reactive species, such as hydroxyl radicals (•OH) and sulfate radicals ($SO_4^{\bullet-}$), capable of mineralizing refractory organic pollutants [4].

Among various oxidants, persulfate (e.g., sodium persulfate, SPS) has attracted considerable interest owing to its high stability, high redox potential, and ability to be activated by heat, UV, or transition metals to produce $SO_4^{\bullet-}$ [5, 6]. For instance, PS can form AOPs systems with Fe^{3+} or Fe^{2+} for phenol degradation [7]. Nevertheless, conventional activation methods, particularly homogeneous Fe^{2+}, often suffer from a narrow applicable pH range (typically acidic conditions), significant iron sludge production, and catalyst deactivation [8-10].

Recently, Fe(VI) has gained attention as a green multifunctional oxidant, offering simultaneous oxidation and coagulation without generating toxic by-products [11]. More importantly, emerging studies suggest that Fe(VI) can synergistically enhance oxidation systems when combined with persulfate [12, 13]. During its reduction, Fe(VI) produces intermediate iron species (Fe(IV)/Fe(V)) and ferric iron (Fe(III)), both of which can effectively activate persulfate to generate $SO_4^{\bullet-}$ and •OH, thereby markedly accelerating contaminant degradation [14, 15].

He and Zhao [16] demonstrated that a Fe(VI)/peroxymonosulfate (PMS) system effectively degraded diclofenac (DCF), with $SO_4^{\bullet-}$, •OH, and high-valent iron species (Fe(IV)/Fe(V)) identified as the main contributors. Comparable reactive species have also been reported in the S(IV)/Fe(VI) system [17]. In addition, reducing agents such as hydroxylamine (HA) have been shown to accelerate the Fe(VI)/persulfate process by promoting the conversion of Fe(III) back to Fe(II) [18].

Guo et al. [19] further found that the electron-donating nature of aniline improved tetracycline degradation by Fe(VI), suggesting that aniline itself may participate in and even facilitate reactions within Fe(VI)-based systems. Jung and Kim [20] optimized the process for aniline degradation using Fe(VI) alone and analysed the intermediate products.

Despite these promising findings, the application of the combined Fe(VI)/persulfate system for aniline degradation remains inadequately explored, with several critical knowledge gaps persisting. Firstly, the synergistic mechanism between Fe(VI) and persulfate (e.g., sodium persulfate (SPS)) is still not fully elucidated. Secondly, the relative contributions of different reactive species (e.g., Fe(IV/V), $SO_4^{\bullet-}$, •OH) are ambiguous. Finally, there is a lack of comprehensive analysis of the degradation pathways under various water chemistry conditions.

To address these research gaps, this study systematically investigates the degradation performance and mechanism of aniline using a combined Fe(VI)/SPS system. We evaluate the effects of critical operational parameters, including SPS dosage, temperature, and pH, on degradation efficiency. Radical quenching experiments are employed to identify the predominant reactive species. Furthermore, liquid chromatography-mass spectrometry (LC-MS) is utilized to identify intermediate products and propose potential degradation pathways. This study aims to provide fundamental mechanistic insights and technical support for the application of Fe(VI)-based AOPs in the treatment of industrial wastewater contaminated with aniline.

2. Materials and Methods

2.1. Chemicals and reagents

All chemicals were of analytical grade and employed as received without additional purification. Aniline ($C_6H_5NH_2$, ≥99.5%), potassium ferrate (K_2FeO_4, ≥96%), sodium persulfate (SPS, $Na_2S_2O_8$, ≥96%), ethanol (EtOH, C_2H_5OH, ≥90%), tert-butanol (TBA, $C_4H_{10}O$, ≥99%), sodium thiosulfate ($Na_2S_2O_3$, ≥99%), hydrochloric acid (HCl, 36 wt.%), sodium hydroxide (NaOH, ≥99%), borax ($Na_2B_4O_7 \cdot 10H_2O$, ≥99%), and potassium hydrogen phthalate ($C_8H_5KO_4$, ≥99.5%) were obtained from commercial sources. All solutions were prepared using deionized water (resistivity = 18.2 MΩ·cm) and stored under appropriate conditions prior to use.

2.2. Aniline degradation experiments

Batch experiments for aniline degradation were conducted in a thermostatically controlled magnetic stirring water bath reactor, as illustrated in Fig. 1. A volume of 250 mL of aniline stock solution (10 mM) was placed in the reactor and mixed with oxidants-Fe(VI) and SPS. The pH and temperature of the reaction system were maintained at preset values using a pH stat controller and the thermostatic water bath, respectively.

Samples were collected at 15-minute intervals and promptly quenched with sodium thiosulfate to terminate the reaction. The quenched samples were filtered through 0.22 μm aqueous syringe filters, diluted as required, and analysed for residual aniline concentration. The degradation kinetics of aniline were investigated using a pseudo-first-order kinetic model. The integrated rate equation is expressed as:

$$lnC_0/C_t = K_{obs} \times t$$

where C_0 (mM) is the initial concentration of aniline, C_t (mM) is the residual concentration of aniline at reaction time t (min), and K_{obs} (min^{-1}) is the observed pseudo-first-order rate constant. The value of K_{obs} quantitatively represents the reaction rate; specifically, it indicates the fractional decrease in aniline concentration per unit time. A higher K_{obs} value corresponds to faster degradation kinetics. The linear regression of $\ln C_0/C_t$ versus t yields K_{obs} as the slope, as applied for the data analysis in Tables 1 and 2.

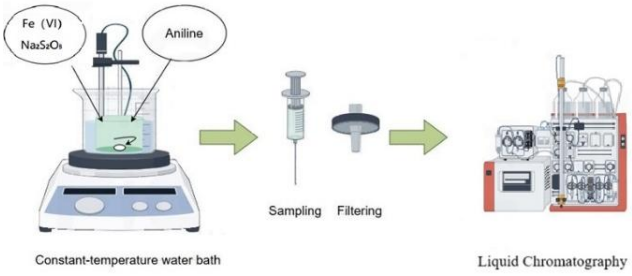

Fig. 1. Apparatus and process for the degradation of aniline.

2.3. Radical quenching experiments

To elucidate the contribution of radical species to aniline degradation, quenching experiments were carried out using excess ethanol (EtOH, for scavenging both •OH and $SO_4^{\bullet-}$[21]) or tert-butanol (TBA, primarily for •OH [22]) at a quencher-to-oxidant molar ratio of 100:1 [23]. The experiments were performed with 10 mM aniline at pH 7 and 30 °C to assess the influence of •OH and $SO_4^{\bullet-}$.

Additionally, the effect of initial pH on aniline removal in the Fe(VI)/SPS system was investigated. Experiments were conducted at 30 °C using 10 mM aniline, 10 mM Fe(VI), and 40 mM SPS, with pH adjusted to 3, 7, 9, and 11. TBA was introduced as a quenching agent. Samples were taken at 15-minute intervals for subsequent analysis. All experiments were performed in triplicate, and the average data is presented with standard deviations.

2.4. Analytical methods

The concentration of residual aniline was measured via high-performance liquid chromatography (HPLC; Agilent 1260 Series, China) fitted with a UV detector operating at 278 nm. A ZORBAX SB-C18 column (4.6 mm × 150 mm, 5 μm) kept at 30 °C was used for analyte separation. The mobile phase, a mixture of methanol and water (60:40, v/v), was pumped at a flow rate of 0.8 mL·min^{-1}. Each injection had a volume of 20 μL, and aniline eluted at approximately 5.2 minutes.

Intermediates produced during the degradation of aniline were characterized by liquid chromatography-mass spectrometry (LC–MS) using a Hypersil Gold column (2.1 mm × 100 mm, 1.9 μm) maintained at 30 °C. The mass spectrometer was run in negative MS2 scan mode with a mass range of m/z 50-500. The mobile phase was a mixture of water (A) and acetonitrile (B) flowing at 0.2 mL·min^{-1}. This method offered a limit of detection (LOD) of 0.08 μg·L^{-1} and a limit of quantification (LOQ) of 0.27 μg·L^{-1}.

3. Results and Discussion

3.1. Comparative degradation of aniline in different systems

The degradation efficiency of aniline by various systems, including Fe(VI) alone, SPS alone, and the combined Fe(VI)/ SPS system, was investigated and the results are presented in Fig. 2. After a 30-minute reaction, the aniline removal rates were 37.78% and 33.21% for the individual Fe(VI) (10 mM) and SPS (40 mM) systems,

respectively. This indicates that both Fe(VI) and SPS can directly react with aniline, albeit to a limited and incomplete extent. In stark contrast, the combined Fe(VI)/SPS system (10 mM / 40 mM) achieved a significantly enhanced removal efficiency of 76.41%. Notably, this value is higher than the arithmetic sum of the efficiencies of the two individual systems (70.99%), providing clear evidence of a synergistic effect between Fe(VI) and SPS.

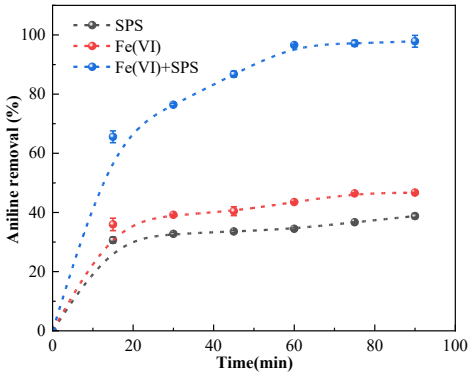

Fig. 2. Comparison of different oxidation systems.

The superior performance of the combined system can be attributed to the activation of SPS by Fe(VI) (Eq. (1)) [24] and its reduction products. Fe(VI) also undergoes self-decomposition (Eq. (2)) [25], While SPS itself is a relatively weak oxidant at ambient temperature, it can be activated to generate powerful sulfate radicals ($SO_4^{\bullet-}$) through various methods, including heat, UV irradiation, and transition metals (Eq. (3)) [6].

However, the significant enhancement observed in the combined system suggests that this direct pathway is not the dominant mechanism. In this system, Fe(VI) serves a dual role: it acts as a potent oxidant itself and, more importantly, as an activator for SPS. It has been reported that Fe(VI) can directly activate SPS via single-electron transfer, producing the persulfate radical ($S_2O_8^{\bullet-}$) and Fe(V) [26, 27]. Furthermore, Fe(VI) is inevitably reduced during the reaction, yielding Fe(III) species [28].

The generated Fe(III), along with Fe(II) produced from the subsequent reactions (e.g., Eq. (4)) [21], can effectively activate SPS [29, 30]. Specifically, Fe(II) efficiently cleaves the peroxo bond of SPS to produce $SO_4^{\bullet-}$, and the interconversion between Fe(III) and Fe(II) establishes a catalytic cycle (Eq. (5)), enabling continuous activation of SPS and sustained generation of reactive radicals [31]. The proposed reactions are summarized as follows:

$$Fe(VI) + S_2O_8^{2-} \rightarrow S_2O_8^{\cdot-} + Fe(V) \quad (1)$$

$$Fe(VI) + H^+ \rightarrow Fe(III) + OH^- \quad (2)$$

$$S_2O_8^{2-} \xrightarrow{\text{heat or Fe（II）}} SO_4^{\cdot-} + SO_4^{2-} \quad (3)$$

$$Fe(III) + S_2O_8^{2-} \rightarrow S_2O_8^{\cdot-} + Fe(II) \quad (4)$$

$$Fe(II) + S_2O_8^{2-} \rightarrow Fe(III) + SO_4^{\cdot-} + SO_4^{2-} \quad (5)$$

3.2. Effect of SPS dosage

To optimize the reaction conditions and gain deeper insights into the synergistic mechanism, the effect of SPS dosage (ranging from 10 to 50 mM) on the degradation efficiency was systematically investigated while keeping the Fe(VI) dosage (10 mM) and initial aniline concentration (10 mM) constant at room temperature (25 ± 2 °C). The results are presented in Figs. 3 (degradation profiles) and 4 (pseudo-first-order kinetic fitting).

As the SPS dosage increased from 10 to 50 mM, the final aniline removal efficiency after 60 minutes significantly improved, rising from approximately 60% to 97.5% (Fig. 3). This indicates that, within the tested concentration range, providing more SPS precursors facilitates more complete degradation of aniline. As listed in Table 1, the apparent reaction rate constant (K_{obs}) of the system increased with the SPS concentration, rising from 0.01413 min^{-1} with 10 mM SPS to 0.06147 min^{-1} with 50 mM SPS. Notably, a significant jump in the K_{obs} value (an increase of approximately 74%) was observed when the Fe(VI) to SPS molar ratio changed from 1:2 to 1:3, after which the rate of increase moderated. This trend is consistent with observations reported for the degradation of other organic compounds by the Fe(VI)/SPS system [32].

The enhancement in degradation kinetics with increasing SPS dosage can be attributed to the promoted generation of reactive radicals, primarily $SO_4^{\bullet-}$ and potentially HO•. This is driven by two parallel and mutually reinforcing pathways: Firstly, a higher SPS concentration provides more substrate for direct activation by Fe(VI) itself (and possibly by the intermediate iron species Fe(V)/Fe(IV)), generating $SO_4^{\bullet-}$ through single-electron transfer reactions. Secondly, it amplifies the Fe(III)/Fe(II) catalytic cycle (Eqs. (4) and (5)), which continuously activate SPS to produce radicals. Therefore, increasing the oxidant concentration is an effective strategy for enhancing the degradation of organic pollutants.

However, excessive SPS dosage can lead to the scavenging of sulfate radicals. When an overabundance of SPS is present, many generated $SO_4^{\bullet-}$ radicals may undergo self-quenching before they can react with the target pollutant (Eqs. (6) and (7)) [33]. The observed slowdown in the rate of K_{obs} increase at 50 mM SPS suggests that such scavenging effects have likely begun to manifest.

$$SO_4^{\cdot-} + SO_4^{\cdot-} \rightarrow 2SO_4^{2-} \quad (6)$$

$$SO_4^{\cdot-} + S_2O_8^{2-} \rightarrow SO_4^{2-} + S_2O_8^{\cdot-} \quad (7)$$

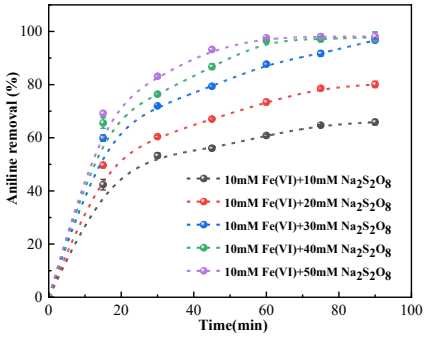

Fig. 3. Effect of SPS dosage.

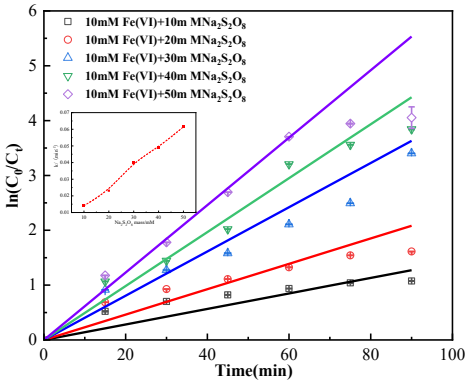

Fig. 4. First-order kinetic model and K_{obs} values for SPS dosage.

Table 1. Proposed first-order reaction kinetic results for SPS dosage.

No.	Fe(VI)+SPS	Linear equation	K_{obs}(min^{-1})	R^2
1	10 mM Fe(VI)+10 mM SPS	y = 0.01413 x	0.01413	0.9912
2	10 mM Fe(VI)+20 mM SPS	y = 0.02313 x	0.02313	0.9661
3	10 mM Fe(VI)+30 mM SPS	y = 0.04034 x	0.04034	0.9912
4	10 mM Fe(VI)+40 mM SPS	y = 0.04917 x	0.04917	0.9940
5	10 mM Fe(VI)+50 mM SPS	y = 0.06147 x	0.06147	0.9937

3.3. Effect of temperature

Reaction temperature is a critical parameter influencing the efficiency of AOPs. The influence of temperature (10-60 °C) on aniline degradation in the Fe(VI)/SPS system was investigated under controlled conditions (pH = 7, $[Aniline]_0$ = 10 mM, $[Fe(VI)]_0$ = 10 mM, $[SPS]_0$ = 40 mM), with the findings illustrated in Figs. 5 and 6. A pronounced enhancing effect of elevated temperature was observed. At the 15-minute mark, the aniline removal efficiency increased dramatically from 52.22% at 10 °C to 92.73% at 60 °C, representing a 77.6% enhancement. These results indicate that increasing the reaction temperature markedly enhances the overall reaction rate. As presented in Fig. 6 and Table 2, the apparent rate constant (K_{obs}) rose steadily with temperature, from 0.02485 min^{-1} at 10 °C to 0.09841 min^{-1} at 60 °C, representing nearly a fourfold increase. This observation is consistent with the trends previously described by Feng et al. [34].

The enhancement can be attributed to multiple temperature-dependent pathways. Firstly, elevated temperature significantly accelerates the thermal decomposition of Fe(VI) itself [35]. The decomposition products, predominantly Fe(III) species, supply the iron source essential for subsequent catalytic cycles. Secondly, heating directly increases the homolytic cleavage rate of SPS. Crucially, both the direct activation of SPS by Fe(VI) and the more sustainable Fe(III)/Fe(II) catalytic activation cycle are endothermic processes. According to the Arrhenius equation ($k = Ae^{(-Ea/RT)}$), increasing the temperature significantly reduces the energy barrier (Ea) for these activation steps. This leads to a substantially higher instantaneous generation rate and steady-state concentration of $SO_4^{\bullet-}$ [34], making a greater number of highly reactive radicals available to attack aniline molecules per unit time. Consequently, the aniline removal efficiency within the first 15 minutes was markedly improved.

In summary, temperature acts as a universal accelerator in the Fe(VI)/SPS system, simultaneously facilitating Fe(VI) decomposition, persulfate activation, and catalytic cycling. These combined effects explain the significantly improved degradation kinetics observed at elevated temperatures.

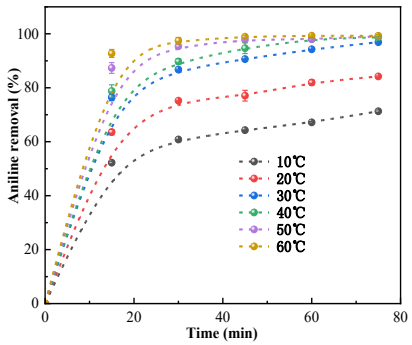

Fig. 5 Effect of temperature.

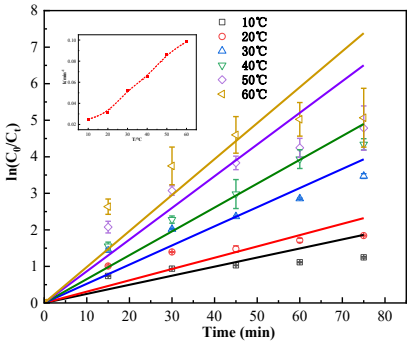

Fig. 6. First-order kinetic model and K_{obs} values for temperature.

Table 2. Proposed first-order reaction kinetic results for temperature.

No.	Temperature (℃)	Linear equation	K_{obs}(min^{-1})	R^2
1	10	y = 0.02485 x	0.02485	0.9633
2	20	y = 0.03094 x	0.03094	0.9040
3	30	y = 0.05242 x	0.05242	0.9859
4	40	y = 0.06529 x	0.06529	0.9718
5	50	y = 0.08671 x	0.08671	0.9605
6	60	y = 0.09841 x	0.09841	0.9010

3.4. Effect of solution pH

Solution pH is a pivotal operational parameter in advanced oxidation processes (AOPs), profoundly influencing the speciation of reactants, the pathways of radical generation, and the overall reaction kinetics. The effect of initial pH (3-11) on the degradation of aniline by the Fe(VI)/SPS system was systematically investigated under controlled conditions (30 °C, [Aniline]$_0$ = 10 mM, [Fe(VI)]$_0$ = 10 mM, [SPS]$_0$ = 40 mM), with the results presented in Fig. 7.

A strong pH-dependent trend in the aniline degradation rate was observed within the first 60 minutes of the reaction, following the order: acidic (pH 3) > neutral (pH 7) > alkaline (pH 11). At the 30-minute mark, the removal efficiencies at pH 3, 7, and 11 were 88.14%, 84.31%, and 82.98%, respectively, indicating a distinct kinetic advantage under acidic conditions. However, upon extending the reaction time to 90 minutes, the final aniline removal efficiencies converged, approaching near-complete degradation across all pH levels. This suggests that pH predominantly modulates the reaction rate rather than the ultimate extent of degradation.

As illustrated in the inset of Fig. 7, Fe(VI) exists primarily in its protonated forms ($H_3FeO_4^+$ and H_2FeO_4) at pH < 4 (Eqs. (8) and (9)) [36]. These species possess a higher standard redox potential ($E^0 \approx +2.20$ V) [37] and exhibit a much stronger direct oxidation capacity towards organic compounds like aniline compared to the deprotonated FeO_4^{2-} species. This accounts for the rapid initial removal observed under acidic conditions.

Furthermore, the decomposition of Fe(VI) in acid is not a single-step process to Fe(III) but proceeds through single-electron transfers, generating transient yet highly reactive intermediate iron species, namely Fe(V) and Fe(IV) (Eq. (10)) [19, 25]. These intermediates possess reactivity orders of magnitude higher than Fe(VI) and can attack organic molecules (R) extremely rapidly (Eqs. (11)-(13)) [19]. The ultimate solid decomposition product of Fe(VI), Fe(III), remains soluble in acidic media [26].

This soluble Fe(III) can effectively activate SPS to produce Fe(II) (albeit with a relatively slow rate constant, $K_{SPS/Fe(III)}$), and the resultant Fe(II) subsequently activates SPS at a very high rate ($K_{SPS/Fe(II)}$ = 27 $M^{-1}s^{-1}$ [13]), leading to the rapid generation of a large flux of $SO_4^{\bullet-}$ radicals. Additionally, some organic reducing intermediates (e.g., semiquinone, hydroquinone) generated during aniline oxidation can reduce Fe(III) back to Fe(II) (Eq. (14)) [38], thereby maintaining and reinforcing this catalytic cycle and providing a sustained source of radicals in the mid-to-late stages of the reaction. In acidic medium, $SO_4^{\bullet-}$ is the stable and dominant radical ($E^0 \approx$ 2.5-3.1 V) [39], which can further transform to •OH in aqueous solution (Eq. (15)) [40], ensuring the highly efficient degradation of aniline.

$$H_2Fe(VI)O_4 + 2H^+ \rightarrow Fe(III) + O_2 + 2H_2O \quad (8)$$

$$Fe(VI) + H_2O \rightarrow Fe(IV) + H_2 \quad (9)$$

$$Fe(VI) \rightarrow Fe(III) + O_2 \uparrow + H_2O_2 \quad (10)$$

$$Fe(VI) + R \rightarrow Fe(V) + R\cdot^+ \quad (11)$$

$$Fe(V) + R \rightarrow Fe(IV) + R\cdot^+ \quad (12)$$

$$Fe(IV) + R \rightarrow Fe(III) + R\cdot^+ \quad (13)$$

$$Fe(III) + Hydroquinone \rightarrow Fe(II) + Semiquinone\cdot + H^+ \quad (14)$$

$$SO_4^{\cdot-} + H_2O \rightarrow \cdot OH + H^+ + SO_4^{2-} \quad (15)$$

In contrast, the reaction pathway shifts significantly as pH increases, resulting in the observed decrease in the initial rate. Under neutral and alkaline conditions, Fe(VI) predominantly exists as FeO_4^{2-}, which has a lower oxidative potential [12]. More critically, Fe(III) begins to hydrolyze at pH > 3 and rapidly forms inactive

ferric hydroxide ($Fe(OH)_3$) precipitates in near neutral and alkaline conditions (Eq. (16)). This precipitate loses its homogeneous catalytic activity, severely impairing the Fe(III)/Fe(II) catalytic cycle. Consequently, the activation of SPS in these pH regimes relies more heavily on the direct activation by initial Fe(VI) and possibly heterogeneous surface reactions on the precipitate.

$$Fe(VI)O_4^{2-} + 3OH^- \rightarrow Fe(OH)_3 \downarrow + 2O_2 \uparrow \quad (16)$$

Despite the differing initial pathways, all systems ultimately contained enough oxidant (40 mM SPS) to achieve complete degradation over an extended period. While the acidic system rapidly consumed the pollutant via efficient catalytic cycles, the neutral and alkaline systems, albeit slower, eventually attained complete degradation through the slow activation of SPS (potentially via homolysis or surface catalysis) and the direct oxidation by Fe(VI), albeit requiring a longer reaction time.

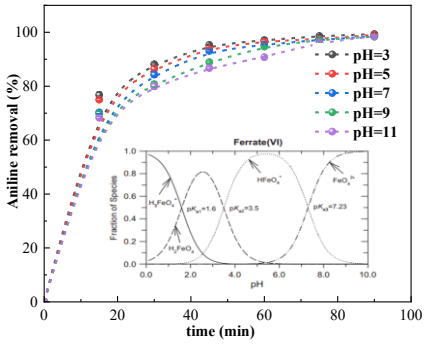

Fig. 7. Effect of the Fe(VI)/SPS system on aniline degradation at different pH values.

3.5. Free radical quenching experiments

To clarify the role of reactive radicals in aniline degradation, quenching tests were performed using ethanol (EtOH) and tert-butanol (TBA) as radical scavengers. As illustrated in Fig. 8(a), under neutral conditions (pH = 7, 30 °C), the presence of EtOH caused a greater reduction in aniline removal efficiency compared to TBA. This difference is attributed to their distinct radical-trapping abilities: EtOH effectively reacts with both sulfate radicals ($SO_4^{\bullet-}$) and hydroxyl radicals (•OH) because of its strong reactivity toward these species, whereas TBA-limited by steric hindrance-primarily quenches •OH but shows much weaker reactivity toward $SO_4^{\bullet-}$ [41, 42], reacts rapidly with •OH but has a comparatively much lower reactivity toward $SO_4^{\bullet-}$. The distinct inhibition effects observed confirm the simultaneous presence and involvement of both $SO_4^{\bullet-}$ and •OH in the Fe(VI)/SPS system [6].

A comparison between the system with TBA and the control system without any quencher (Fig. 8(c)) further revealed that aniline removal was not completely suppressed. This indicates that non-radical pathways, specifically the direct electron transfer oxidation by Fe(VI) itself, also contribute significantly to the degradation process. The contribution of radical-based oxidation was found to be highly pH-dependent.

Quantitative analysis of the quenching effects suggested that •OH played a substantial role, accounting for approximately 50% of the degradation at pH=3. Its contribution decreased to about 20% at neutral pH (pH=7) and fell below 20% under alkaline conditions (pH=11). This trend indicates a decrease in the generation and/or utilization of •OH as pH increases. Conversely, under alkaline conditions, Fe(VI) itself is more stable.

More importantly, the intermediate iron species (Fe(IV)/Fe(V)) generated from its reduction possess reactivities far exceeding that of Fe(VI) [34] and become the dominant oxidizing agents for aniline degradation. Notably, despite the varying dominant mechanisms across the pH range, near-complete aniline removal was achieved after 90 minutes in all cases (Fig. 7), demonstrating the system's robustness. The degradation pathways can be summarized as follows:

Under acidic conditions (pH=3), The process involves multiple concurrent mechanisms, including direct oxidation by Fe(VI), attack by highly reactive intermediate iron species (Fe(IV)/Fe(V)), and radical-based oxidation (primarily by $SO_4^{\bullet-}$, which subsequently generates •OH) driven by an efficient soluble Fe(III)/Fe(II) catalytic cycle activating SPS.

In neutral and alkaline media, the contribution of radical species changes. Because sulfate radicals ($SO_4^{\bullet-}$) have a considerably longer lifetime (30-40 μs) than hydroxyl radicals (•OH, ~20 ns) [15], they play a more dominant role in diffusion and reactions with organic compounds. Nevertheless, the main oxidation pathways increasingly rely on direct electron transfer by Fe(VI) and, more critically, on the highly reactive intermediate species Fe(IV) and Fe(V). This shift occurs because the homogeneous Fe(III)/Fe(II) redox cycle is suppressed by the precipitation of ferric hydroxides under these pH conditions.

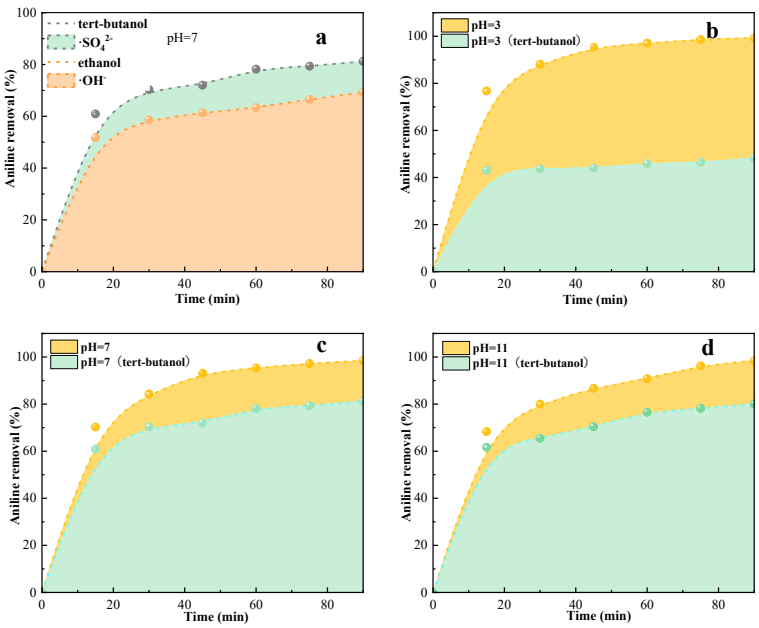

Fig. 8. Comparison of the effects of radical quenchers on aniline degradation under different pH.

3.6. Proposed degradation mechanism of aniline by the Fe(VI)/SPS system

To further clarify the reaction mechanism of aniline degradation in the Fe(VI)/SPS system, liquid chromatography-mass spectrometry (LC–MS) was employed to identify transformation intermediates. Fourteen major intermediates were detected (Fig. 9). These findings demonstrate that the cooperative action of Fe(VI) and SPS not only enhances the generation of reactive radicals ($SO_4^{\bullet-}$ and •OH) but also establishes a complex reaction network. This network involves direct oxidation by Fe(VI), high-valent iron species (Fe(IV)/Fe(V)), and radical formation through the Fe(II)/SPS activation pathway.

The identified intermediates, including nitrobenzene, azobenzene, and p-benzoquinone, are partially consistent with previous findings by Jung and Kim [20] using GC-MS. Furthermore, the oxidation pathways, involving hydroxylation, ring-opening, and coupling reactions, align with studies on other compounds, such as the oxidation of Butylated Hydroxyanisole initiated by Fe(VI)/PMS as reported by Shi et al. [43]. Based on the intermediate products, a three-stage degradation process for aniline is proposed:

Stage I: Initial Oxidation and Radical Formation. The aniline molecule (A1) undergoes initial attack, forming an aniline radical cation. This can occur via direct single-electron transfer oxidation by Fe(VI) (generating Fe(V)) or through hydrogen abstraction/electron transfer by $SO_4^{\bullet-}$/•OH.

Stage II: Series of Degradation Reactions. The subsequent reactions proceed through four primary pathways:

- **Path 1 (Hydroxylation and Quinone Formation).** The benzene ring of aniline (A1) is hydroxylated by radicals or high-valent iron species, yielding aminophenol (A2, $C_6H_4NH_2OH$). This is further oxidized via deamination to form hydroquinone/catechol (A3, $C_6H_4(OH)_2$), and finally to p-benzoquinone (A4, $C_6H_4O_2$) and its derivatives, preceding ring cleavage.
- **Path 2 (Nitro-Group Formation).**The attack on the amino group by $SO_4^{\bullet-}$/•OH or high-valent iron species leads to dehydrogenation, forming nitrosobenzene (A5, C_6H_5NO), which is subsequently oxidized to nitrobenzene (A6, $C_6H_5NO_2$) and further to nitrophenols (A7, $NO_2C_6H_4OH$) [20].
- **Path 3 (Coupling and Subsequent Reactions).** Aniline radical intermediates ($C_6H_5NH^{\bullet}$) undergo coupling reactions to form azobenzene (A8, $C_{12}H_{10}N_2$). The benzene ring of the coupled product can be further attacked (e.g., nitration) to form nitroazobenzene (A9, $C_{12}H_9N_3O_2$). $SO_4^{\bullet-}$ can initiate such coupling reactions in aromatic compounds via electron transfer [24]. These coupled products eventually undergo ring-opening.
- **Path 4 (C-C Coupling):** The aniline radical intermediate ($C_6H_5NH^{\bullet}$, electrophile) couples with a neutral aniline molecule (nucleophile) at the para-position, generating 4-aminodiphenylamine (A11, $(C_6H_4)_2(NH_2)_2$).

Stage III: Ring-Opening and Mineralization. Intermediates such as A10, A12, and A13 are identified as ring-opening products (e.g., small molecular carboxylic acids like maleic acid). These compounds are subsequently broken down into smaller molecules (A14, A15) and ultimately mineralized to CO_2 and H_2O. The nitrogen element is primarily converted into nitrate (NO_3^-) and/or ammonium (NH_4^+).

In summary, the Fe(VI)/SPS coupled system effectively regulates toxicity during the degradation process. While toxic intermediates like nitrosobenzene and 4-aminodiphenylamine may form initially, they are progressively transformed through continuous oxidation and ring-opening reactions into low-toxicity carboxylic acids and, finally, innocuous inorganic products (CO_2, H_2O, NO_3^-, NH_4^+). The multi-stage transformation characteristics, particularly the effective control of ecotoxic aromatic amine intermediates through deep oxidation as observed in the pH experiments (Section 3.4), indicate a toxicity attenuation feature, especially under acidic conditions (pH=3).

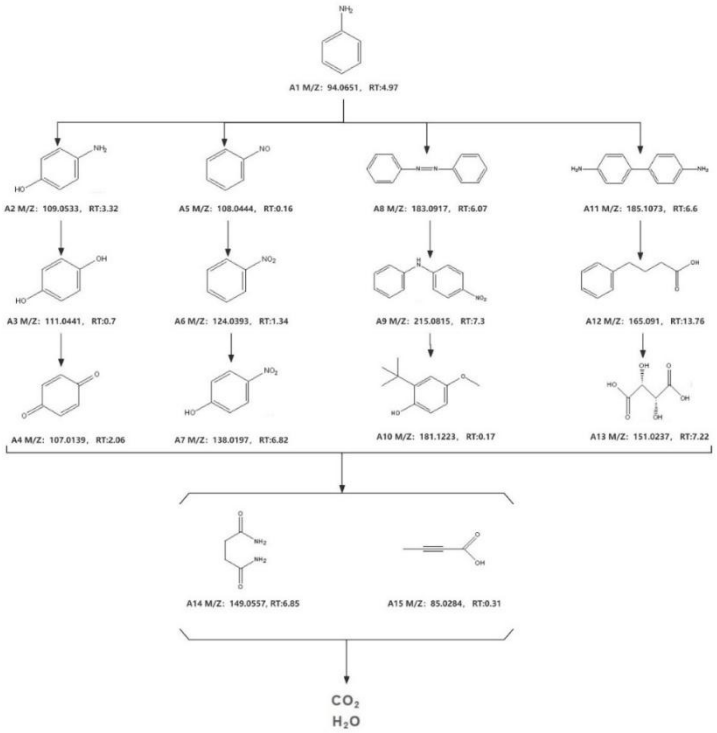

Fig. 9. Degradation path of aniline in potassium ferrate sodium persulfate system.

4. Conclusion

This study demonstrates that the combined Fe(VI)/SPS system efficiently degrades aniline in aqueous solution. Under optimal conditions (pH = 3, 30 °C, Fe(VI):SPS = 10 mM: 40 mM), an aniline removal efficiency of 88.14% was achieved within 30 min, significantly higher than that of individual Fe(VI) (37.78%) or SPS (33.21%) systems, exhibiting a clear synergistic effect (combined efficiency exceeded the arithmetic sum of separate systems).

Increasing the SPS dosage from 10 to 50 mM enhanced the removal efficiency after 60 min from 60% to 97.5%, with the apparent reaction rate constant (K_{obs}) increasing from 0.01413 min^{-1} to 0.06147 min^{-1}. Elevated temperature (10 to 60 °C) markedly accelerated the reaction, increasing K_{obs} nearly fourfold (0.02485 to 0.09841 min^{-1}). Quenching experiments revealed that both $SO_4^{\bullet-}$ and •OH

contributed significantly to degradation under acidic conditions (with •OH accounting for ∼50%), whereas under alkaline conditions, high-valent iron species (Fe(IV)/Fe(V)) dominated the oxidation process.

Intermediate analysis indicated that aniline was degraded through multiple pathways, including hydroxylation, nitration, and coupling reactions, ultimately leading to mineralization into inorganic products. The innovation of this work lies in elucidating the synergy and competition between radical and non-radical pathways in the Fe(VI)/SPS system, providing quantitative kinetic evidence under key operational parameters, and offering a theoretical basis for the application of this technology in treating wastewater containing highly toxic organic compounds.

Nomenclatures

C_o	The Initial Concentration, mM
C_t	The Residual Concentration, mM
K_{obs}	The Rate constant, min^{-1}

Abbreviations

AOPs	Advanced Oxidation Processes
DCF	Diclofenac
Fe(VI)	Ferrate
IARC	International Agency for Research on Cancer
LC-MS	Liquid Chromatography–Mass Spectrometry
PMS	Peroxymonosulfate
SPS	Sodium Persulfate
UV	Ultraviolet

References

1. Chaturvedi, N.K.; and Katoch, S.S. (2020). Remedial technologies for aniline and aniline derivatives elimination from wastewater. *Journal of Health & Pollution*, 10(25), 1-11.
2. Wang, X.; Wang, Y.; Shu, Z.; Cao, Y.; Wang, X.; Zhou, F.; and Huang, J. (2023). Phenolic hydroxyl-functionalized hyper-cross-linked polymers for efficient adsorptive removal of aniline. *Separation and Purification Technology*, 305, 122443.
3. Wu, N.-P.; Zhang, Q.; Tan, B.; Li, M.; Lin, B.; He, J.; Su, J.-H.; and Shen, H.-N. (2023). Integrated fixed-film activated sludge systems in continuous-flow and batch mode acclimated from low to high aniline concentrations: Performance, mechanism and metabolic pathways. *Bioresource Technology*, 379, 129043.
4. Liu, Y.; Liu, L.; and Wang, Y. (2021). A critical review on removal of gaseous pollutants using sulfate radical-based advanced oxidation technologies. *Environmental Science & Technology*, 55(14), 9691-9710.
5. Dong, L.; Xia, Y.; Hu, Z.; Zhang, M.; Qiao, W.; Wang, X.; and Yang, S. (2024). Research progress of persulfate activation technology. *Environmental Science and Pollution Research*, 31(22), 31771-31786.

6. Derbalah, A.; and Sakugawa, H. (2024). Sulfate radical-based advanced oxidation technology to remove pesticides from water a review of the most recent technologies. *International Journal of Environmental Research*, 18(1), 11.
7. You, Y.; and He, Z. (2023). Phenol degradation in iron-based advanced oxidation processes through ferric reduction assisted by molybdenum disulfide. *Chemosphere*, 312, 137278.
8. Tang, Z.; Xu, C.; Shen, C.; Sun, S.; Meng, X.-Z.; Wang, S.; and Li, F. (2024). Evaluation of key intermediates in azo dye degradation by advanced oxidation processes: Comparing anilines and phenols. *ACS ES&T Water*, 4(11), 4872-4880.
9. Manna, M.; and Sen, S. (2023). Advanced oxidation process: A sustainable technology for treating refractory organic compounds present in industrial wastewater. *Environmental Science and Pollution Research*, 30(10), 25477-25505.
10. Velo-Gala, I.; López-Peñalver, J.J.; Sánchez-Polo, M.; and Rivera-Utrilla, J. (2014). Comparative study of oxidative degradation of sodium diatrizoate in aqueous solution by H_2O_2/Fe^{2+}, H_2O_2/Fe^{3+}, Fe (VI) and UV, H_2O_2/UV, $K_2S_2O_8$/UV. *Chemical Engineering Journal*, 241, 504-512.
11. Yu, J.; Sumita; Zhang, K.; Zhu, Q.; Wu, C.; Huang, S.; Zhang, Y.; Yao, S.; and Pang, W. (2023). A review of research progress in the preparation and application of ferrate (VI). *Water*, 15(4), 699.
12. Zhang, X.; Zhu, X.; Li, H.; Wang, C.; and Zhang, T. (2023). Combination of peroxymonosulfate and Fe(VI) for enhanced degradation of sulfamethoxazole: The overlooked roles of high-valent iron species. *Chemical Engineering Journal*, 453, 139742.
13. Li, D.; Chen, D.; Yao, Y.; Lin, J.; Gong, F.; Wang, L.; Luo, L.; Huang, Z.; and Zhang, L. (2016). Strong enhancement of dye removal through addition of sulfite to persulfate activated by a supported ferric citrate catalyst. *Chemical Engineering Journal*, 288, 806-812.
14. Dinc, O.; Wacławek, S.; Solís, R.R.; and Dionysiou, D.D. (2024). Synergistic oxidative removal of sulfamethoxazole using Ferrate(VI) and peroxymonosulfate. *Chemical Engineering Journal*, 488, 151085.
15. Delavaran Shiraz, A.; Takdastan, A.; and Borghei, S.M. (2018). Photo-Fenton like degradation of catechol using persulfate activated by UV and ferrous ions: Influencing operational parameters and feasibility studies. *Journal of Molecular Liquids*, 249, 463-469.
16. He, H.; and Zhao, J. (2023). The efficient degradation of diclofenac by ferrate and peroxymonosulfate: Performances, mechanisms, and toxicity assessment. *Environmental Science and Pollution Research*, 30(5), 11959-11977.
17. Chen, K.; Cui, Z.; Zhang, Z.; Pang, H.; Yang, J.; Huang, X.; and Lu, J. (2022). Life-sustaining of H^+ in S(IV)/Fe(VI) system for efficient removal of dimethoate in water: Active species identification and mechanism. *Chemical Engineering Journal*, 445, 136865.
18. Li, C.; Lin, H.; Armutlulu, A.; Xie, R.; Zhang, Y.; and Meng, X. (2019). Hydroxylamine-assisted catalytic degradation of ciprofloxacin in ferrate / persulfate system. *Chemical Engineering Journal*, 360, 612-620.
19. Guo, J.; Wang, S.; Li, T.; Wang, L.; and You, H. (2024). A new perspective on contaminants as "activators": Aromatic amine groups promoted

degradation of tetracycline by ferrate(VI). *Journal of Hazardous Materials*, 479, 135740.

20. Jung, S.-Y.; and Kim, I.-K. (2018). Degradation of aniline by liquid ferrate(VI). *Desalination and Water Treatment*, 136, 245-251.
21. Yang, F.; Yin, C.; Zhang, M.; Zhu, J.; Ai, X.; Shi, W.; and Peng, G. (2022). Enhanced Fe(III)/Fe(II) redox cycle for persulfate activation by reducing sulfur species. *Catalysts*, 12(11), 1435.
22. Liu, W.; Liu, Y.; Xiong, Y.; Xiao, X.; Liu, C.; Yuan, B. and Pu, X. (2023). Performances and mechanisms of ferrate(VI) oxidation process for shale gas flowback water treatment. *Process Safety and Environmental Protection*, 173, 120-130.
23. Sheikhi, S.; Jebalbarezi, B.; Dehghanzadeh, R.; Maryamabadi, A.; and Aslani, H. (2022). Sulfamethoxazole oxidation in secondary treated effluent using Fe(VI)/PMS and Fe(VI)/H_2O_2 processes: Experimental parameters, transformation products, reaction pathways and toxicity evaluation. *Journal of Environmental Chemical Engineering*, 10(3), 107446.
24. Laftani, Y.; Chatib, B.; Hachkar, M.; and Boussaoud, A. (2025). Exploring the reactivity of hydroxyl and sulfate radicals in enhancing water decontamination processes. *International Journal of Environmental Science and Technology*, 22(14), 14719-14728.
25. Zhu, J.; Yu, F.; Meng, J.; Shao, B.; Dong, H.; Chu, W.; Cao, T.; Wei, G.; Wang, H.; and Guan, X. (2020). Overlooked role of Fe(IV) and Fe(V) in organic contaminant oxidation by Fe(VI). *Environmental Science & Technology*, 54(15), 9702-9710.
26. Sharma, V.K. (2013). Ferrate(VI) and Ferrate(V) oxidation of organic compounds: Kinetics and mechanism. *Coordination Chemistry Reviews*, 257(2), 495-510.
27. Huang, Z.-S.; Wang, L.; Liu, Y.-L.; Zhang, H.-Y.; Zhao, X.-N.; Bai, Y.; and Ma, J. (2021). Ferrate self-decomposition in water is also a self-activation process: Role of Fe(V) species and enhancement with Fe(III) in methyl phenyl sulfoxide oxidation by excess ferrate. *Water Research*, 197, 117094.
28. Fan, W.-Y.; Zhang, X.; Guo, P.-C.; and Sheng, G.-P. (2023). Highly efficient removal of phosphonates by ferrate-induced oxidation coupled with in situ coagulation. *Journal of Hazardous Materials*, 451, 131104.
29. Liang, J.; Duan, X.; Xu, X.; Chen, K.; Wu, F.; Qiu, H.; Liu, C.; Wang, S.; and Cao, X. (2021). Biomass-derived pyrolytic carbons accelerated Fe(III) / Fe(II) redox cycle for persulfate activation: Pyrolysis temperature-depended performance and mechanisms. *Applied Catalysis B*: *Environmental*, 297, 120446.
30. Mo, J.; Lin, T.; Zhang, X.; Jiang, F.; and Chen, H. (2023). Effects of Fe(II)-activated persulfate/sodium percarbonate (PS/SPC) pretreatment on ultrafiltration membrane fouling control and mechanisms. *Desalination*, 547, 116258.
31. Giannakis, S.; Lin, K.-Y.A.; and Ghanbari, F. (2021). A review of the recent advances on the treatment of industrial wastewaters by Sulfate Radical-based Advanced Oxidation Processes (SR-AOPs). *Chemical Engineering Journal*, 406, 127083.

32. Li, S.-X.; Wei, D.; Mak, N.-K.; Cai, Z.; Xu, X.-R.; Li, H.-B.; and Jiang, Y. (2009). Degradation of diphenylamine by persulfate: Performance optimization, kinetics and mechanism. *Journal of Hazardous Materials*, 164(1), 26-31.
33. Zhang, Y.; Chen, W.; Xu, L.; Pi, J.; and Wang, M. (2023). New insights into the conversion of acetic acid in sodium aluminate solutions by AOPs. *Journal of Sustainable Metallurgy*, 9(4),1691-1703.
34. Feng, M.; Cizmas, L.; Wang, Z.; and Sharma, V.K. (2017). Synergistic effect of aqueous removal of fluoroquinolones by a combined use of peroxymonosulfate and ferrate(VI). *Chemosphere*, 177, 144-148.
35. Xie, J.; Li, B.; Liu, H.; Li, Y.; He, J.-B.; Zheng, Y.; Lau, K.-C.; and Lau, T.-C. (2021). Hydrogen atom transfer in the oxidation of alkylbenzenesulfonates by Ferrate(VI) in aqueous solutions. *Dalton Transactions*, 50(2), 715-721.
36. Lalthazuala, L.; Lalhmunsiama, L.; Vanlalhmingmawia, C.; Tiwari, D.; Choi, S.S.; and Lee, S.-M. (2022). Newer insights on Ferrate(VI) reactions with various water pollutants: A review. *Applied Chemistry for Engineering*, 33(3), 258-271.
37. Cao, J.-Y.; Du, Y.; Dai, X.; Liu, T.; Wang, Z.-J.; Li, J.; Zhang, H.; Zhou, P.; and Lai, B. (2024). Ferrate(VI)-based synergistic oxidation processes (Fe(VI)-SOPs): Promoted reactive species production, micropollutant/microorganism elimination, and toxicity reduction. *Chemical Engineering Journal*, 489, 151180.
38. Chai, J.; Yu, W.; Kong, H.; Liu, H.; Li, Z.; Huang, J.; Pi, R.; Yang, Z.; and Sun, X. (2025). Synergistic and continuous driving of Fe(III)/Fe(II) cycle by electron-rich organic contaminants and peroxymonosulfate: Homogeneous feasibility and heterogeneous application. *Chemical Engineering Journal*, 525,170736.
39. Mei, Q.; Sun, J.; Han D.; Wei, B.; An, Z.; Wang, X.; Xie, J.; Zhan, J.; and He, M. (2019). Sulfate and hydroxyl radicals-initiated degradation reaction on phenolic contaminants in the aqueous phase: Mechanisms, kinetics and toxicity assessment. *Chemical Engineering Journal*, 373, 668-676.
40. Xie, X.; Zhang, Y.; Huang, W.; and Huang, S. (2012). Degradation kinetics and mechanism of aniline by heat-assisted persulfate oxidation. *Journal of Environmental Sciences*, 24(5), 821-826.
41. Wang, J.; Li, Y.; Yang, J.; Feng, Z.; Jing, K.; Guo, K.; and Zhang, G. (2024). Oxidation of selected fluoroquinolones by ferrate(VI) in water: Kinetics, mechanism, effects of constituents, and reaction pathways. *Environmental Research*, 243, 117845.
42. Lee, Y.; Kissner, R.; and von Gunten, U. (2014). Reaction of Ferrate (VI) with ABTS and self-decay of ferrate (VI): Kinetics and mechanisms. *Environmental Science & Technology*, 48(9), 5154-5162.
43. Shi, P.; Yue, X.; Teng, X.; Qu, R.; Rady, A.; Maodaa, S.; Allam, A.A.; Wang, Z.; and Huo, Z. (2024). Degradation of butylated hydroxyanisole by the combined use of peroxymonosulfate and Ferrate(VI): Reaction kinetics, mechanism and toxicity evaluation. *Toxics*, 12(1), 54.